

Studying High Redshift Galaxy Clusters with the ESO Distant Cluster Survey

G. RUDNICK¹, S. WHITE¹, A. ARAGÓN-SALAMANCA², R. BENDER^{3,4}, P. BEST⁵, M. BREMER⁶, S. CHARLOT^{1,7}, D. CLOWE⁸, J. DALCANTON⁹, M. DANTEL¹⁰, G. DE LUCIA¹, V. DESAI⁹, B. FORT⁷, C. HALLIDAY¹¹, P. JABLONKA¹⁰, G. KAUFFMANN¹, Y. MELLIER⁷, B. MILVANG-JENSEN⁴, R. PELLO¹², B. POGGIANTI¹¹, S. POIRIER¹⁰, H. ROTTGERING¹³, R. SAGLIA³, P. SCHNEIDER⁸, L. SIMARD¹⁴, D. ZARITSKY¹⁵

¹MPA, Garching, Germany, ²University of Nottingham, UK, ³Ludwig-Maximilian University, Munich, Germany, ⁴MPE, Munich, Germany, ⁵ROE, Edinburgh, UK, ⁶University of Bristol, UK, ⁷IAP, Paris, France, ⁸IAEF, University of Bonn, Germany, ⁹University of Washington, Seattle, USA, ¹⁰OPM, Paris, France, ¹¹Osservatorio Astronomico di Padova, Padova, Italy, ¹²OMP, Toulouse, France, ¹³Leiden Observatory, The Netherlands, ¹⁴HIA, Victoria, Canada, ¹⁵Steward Observatory, Tucson, USA

Galaxy clusters are the most massive quasi-equilibrium objects in the Universe and are the meeting places of the cosmos. Their deep potential wells are dominated by unseen dark matter, but contain a cosmologically representative baryon fraction in the form of galaxies and intergalactic gas. These are trapped in a virialized state, with the gas heated to tens of millions of degrees and the galaxies moving with *rms* velocities of ~ 1000 kms $^{-1}$.

The study of the evolution of galaxy clusters and of the galaxies within them has largely been driven by observation. Starting in the late 1970's a picture began to emerge in which cluster galaxies evolve towards redder colours with decreasing redshift (Butcher & Oemler 1978) and in which galaxy morphologies are biased towards ellipticals and bulge-dominated systems in denser environments (Dressler 1980). In the following years, imaging with the Hubble Space Telescope (HST) and spectroscopy with 4-meter class and larger telescopes confirmed and extended these early results, adding detailed information about the spectral and morphological properties of galaxies out to $z \sim 0.5$.

A theoretical framework has developed for interpreting these observations, based largely on simulations of dynamical effects on cluster galaxies. As galaxies fall into clusters along the filaments which define large-scale structure, the observed trends can be imprinted by a variety of processes: galaxy morphologies may be altered by repeated gravitational shocking through high speed encounters with other galaxies and with the global cluster potential (galaxy harassment; e.g. Farouki & Shapiro 1981; Moore et al 1996); hot gas envelopes around galaxies can be removed by the hot intra-cluster medium, eliminating the reservoir of gas

which can accrete onto the disk and form stars (strangulation; e.g. Larson, Tinsley & Caldwell 1980); the HI can be similarly stripped by motion through the intra-cluster medium (ram-pressure stripping; e.g. Gunn & Gott 1972) or may be used up in a brief star-burst triggered by the high pressure cluster environment (stimulated star formation; e.g. Dressler & Gunn 1983); and massive galaxies may merge into a central supergiant cD (cannibalism; White 1976). Theoretical treatments of these processes have improved dramatically as computer capabilities have advanced. Dark matter simulations can follow the formation of rich clusters, tracking the evolution of substructures as small as the halos of the faintest dwarf galaxies. The formation of the galaxies themselves can then be studied by adding simplified treatments of gas cooling, star formation, feedback, and stellar evolution (e.g. Springel et al. 2001).

The wealth of observations now available suggests that none of these processes dominates the transformation of galaxies; all appear to play some role, and they may have differing importance in different environments. Their interplay makes clusters ideal laboratories for studying galaxy evolution. This usefulness is enhanced by several practical advantages. Clusters contain many galaxies close together on the sky and at the same redshift, making efficient observation easy with a modest field of view and permitting the approximation that all cluster members are equidistant from the observer.

One of the limitations in using existing observations to constrain theoretical models is that most studies of clusters at $z > 0.3$ have concentrated on X-ray selected samples. This biases the samples towards the most massive and the densest systems. In addition, the

largest available sample at $z \sim 0.4\text{--}0.5$ has heterogeneous and poorly defined selection criteria, significantly complicating any comparison with theoretical predictions. Finally, few clusters have been observed *in detail* at $z \geq 0.5$ where evolutionary changes become dramatic.

The time is ripe to significantly advance our understanding of galaxy evolution in clusters. The basic theoretical paradigm for structure formation is now well established on the relevant scales, and many of the important physical processes can be calculated reliably. Even more importantly, improved instrumental capabilities allow quite precise data on the structure and stellar content of galaxies to be obtained out to redshifts where evolutionary effects are large — at $z \sim 0.8$ where the universe was less than half as old as it is today.

The ESO Distant Cluster Survey

We initiated the **ESO Distant Cluster Survey** (EDisCS), an ESO Large Programme, to take the next step in surveying the evolution of clusters and cluster galaxies. We aim to make a systematic study of cluster structure and cluster galaxies out to $z \sim 0.8$ at a level of detail which will allow quantitative comparison with the large and statistically complete samples of nearby clusters being provided by the 2dF and, particularly, the SDSS projects. Our programme involves matched optical photometry from the VLT and near-IR photometry from the NTT, followed up by multi-object spectroscopy using FORS2 on the VLT. Science goals for the photometric part of the survey include: characterizing the absolute rest-frame ultraviolet (UV) to near infrared (NIR) spectral energy distributions (SEDs) of the galaxies; studying galaxy morphology as a function of SED; measuring the

cluster luminosity functions as a function of redshift and of cluster properties; estimating cluster masses through gravitational lensing; and characterising cluster structure. In practice, this involves deep, high resolution imaging of a large enough cluster sample to span the (large) expected variance in cluster properties, the use of bulge-disk decomposition software to quantify galaxy morphology and of photometric redshifts to reject non-members, and the careful analysis of faint image shapes to measure the gravitational shear.

Our follow-up spectroscopy targets a second set of science goals: measuring the stellar and dynamical masses of cluster galaxies; characterizing their chemical abundances, star formation rates (SFRs) dust contents, and star formation histories (SFHs); comparing these with the properties of field galaxies at the same redshift; and studying the dynamical structure of the clusters. These require high quality spectra for many member galaxies in each cluster and with well understood sampling and completeness statistics. Only with a dataset of this quality is a realistic confrontation with theoretical models possible. Our consortium has already carried out suites of high resolution simulations of the formation of clusters and cluster galaxies which can be used to investigate whether the physical processes outlined above can, in some combination, account for the properties we observe for galaxies in our EDisCS sample.

ESO's suite of instruments and telescopes is ideally suited for such a project, which requires optical and NIR imagers with excellent image quality and relatively wide fields, as well as an efficient multi-object spectrograph mounted on an 8-meter class telescope.

Survey Description and Progress

To ensure the most efficient use of telescope time, successive refinement steps were taken to arrive at a robust cluster sample. An original set of 30 cluster candidates, 15 with estimated redshifts $z \sim 0.5$ and 15 with $z \sim 0.8$, was drawn from the optically selected Las Campanas Distant Cluster Survey (LCDCS; Gonzalez et al. 2001). Given that the spurious candidate rate in the LCDCS can be as high as 50% by $z \sim 0.8$, we used four nights on VLT/FORS2 to obtain two-colour images of each field to confirm the presence of a galaxy overdensity with the expected elliptical-like colours. We then chose the 10 best cluster candidates at each estimated redshift for deeper imaging, followed by spectroscopy. These 20 clusters were observed at the VLT in *BVI* for the $z \sim 0.5$ candidates and *VRI* for the $z \sim 0.8$ candidates. In addition, 20 nights of NIR observations were scheduled at the New Technology Telescope (NTT) using the SOFI NIR camera. This time was used to get K_s -band data for the $z \sim 0.5$ candidates and JK_s for the $z \sim 0.8$ candidates. At the present time, all of the

optical and all but one night of the NIR imaging is complete. Most of the data were taken under excellent conditions with almost all combined images having $<1.0''$ FWHM seeing. In Figure 1 we show optical images for four of our clusters. *I*-band selected catalogues with multi-band photometry were then constructed using the SExtractor software (Bertin & Arnouts 1996). The optical and NIR imaging, including the construction of the catalogues, will be described in upcoming papers (White et al., in preparation; Aragón-Salamanca et al., in preparation).

An initial phase of spectroscopy consisted of a relatively short exposure of a single mask in each field to confirm the presence of a true cluster in the expected redshift range. This resulted in the elimination of one high-redshift candidate that appeared to be a superposition of several weak groups. We then began taking longer exposures of 3 or 4 masks per cluster with the aim of obtaining high quality spectra for ~ 50 members in each cluster. As of April 2003 we have observed for 19 of our total allocated 22 nights (the eight nights of data from Spring 2002 are fully reduced), confirming that all extensively observed clusters are indeed real. Our final sample will have 7 clusters with true redshifts in the range $0.6 \leq z \leq 0.8$. We now have 1240 redshifts for our high redshift clusters, and 554 for our low redshift clusters. We project, given our performance for the first eight

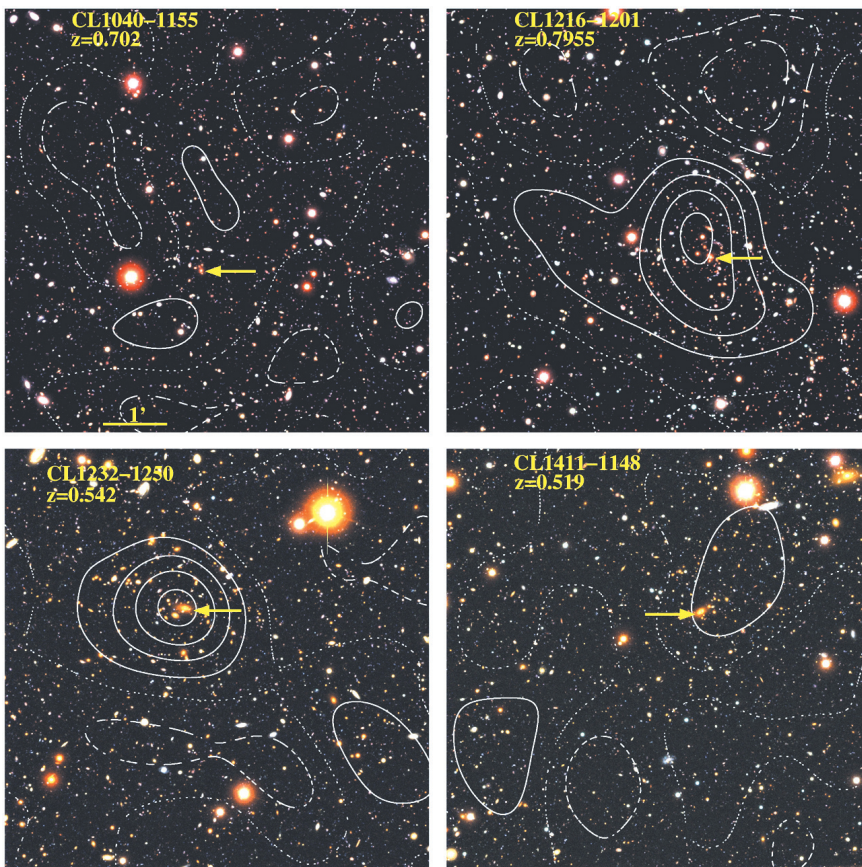


Figure 1: 3-colour images with overlaid weak lensing mass maps for four of the clusters in the EDisCS sample. The top two images, cl1040-1155 on the left and cl1216-1201 on the right, are from the high-redshift sample and were imaged in *I*, *R*, and *V*. The bottom two images, cl1232-1250 on the left and cl1411-1148 on the right, are from the intermediate-redshift sample and were imaged in *I*, *V*, and *B*. The yellow arrow in each frame indicates the location of the BCG. The weak lensing mass maps are normalized to have zero mean surface density at the edge of the images, with the solid contours indicating positive density, the dotted contour zero density, and the dashed contours negative density. Each contour represents a change in surface mass density of about $10^{-8} (h_{70})^{-1} M_\odot / kpc^2$ in an $\Omega_m = 0.3$, $\Lambda = 0.7$ cosmology. All of these clusters have been spectroscopically confirmed with many members, but some of them show no associated peak in their weak lensing mass distribution, demonstrating the diversity of the relation between light and mass in our cluster sample. Figure prepared by Douglas Clowe.

nights, that we now have at least 380 cluster members for the high redshift fields and at least 200 cluster members for the intermediate redshift fields. After the remaining three nights of our allotted spectroscopy, we should reach final numbers of 1290/410 at high redshift and 1000/350 at intermediate redshift. The spectroscopic data will be presented in Halliday et al. (in preparation).

At the present time we already have an impressive data set, with extensive photometry over a long baseline in wavelength, a set of 19 fully confirmed clusters at $0.4 < z < 0.8$ with a range in cluster richness, and fully reduced spectroscopy of about 920 galaxies (from our spectroscopy in 2002). We are, however, still far from being spectroscopically complete even at bright magnitudes. We remove non-members from our photometric samples in two steps, first by using photometric redshifts calculated with two independent codes (Rudnick et al. 2001; Hyperz - Bolzonella, Miralles, & Pelló 2000); then through statistical subtraction of the remaining background within a physical projected radius, $r_{clust} = 0.75 (h_{70})^{-1}$ Mpc, using the observed population density at larger clustercentric distance. Our photometric redshifts z_{phot} are quite accurate, with $\langle |z_{spec} - z_{phot}| \rangle = 0.06 - 0.08$ for both the $z \sim 0.5$ and $z \sim 0.8$ clusters. Using our photometric redshifts we reject $\sim 60\%$ of the field galaxies above the spectroscopic limit and 75-80% of the field galaxies brighter than $I = 25$, while retaining $\sim 90\%$ of all confirmed cluster members, independent of rest-frame colour. The subsequent statistical subtraction removes $\sim 50\%$ of the remaining galaxies. The performance of these techniques will be evaluated in detail in Pelló et al. (in preparation).

The Cluster Luminosity Function and its Evolution

One important observational characteristic of a galaxy population is its luminosity function (LF), which describes the galaxy abundance as a function of absolute magnitude. Evolution of the LF encodes how the luminosity distribution of a galaxy population evolves as a result of star formation, of stellar aging, of obscuration, and of galaxy merging. Observations of the structure and kinematics of cluster ellipticals show that their stellar mass-to-light ratios have increased by about a factor of 2.5 in the B -band since $z = 1$, presumably a result of the aging of their stars. For mixed populations, however, the fading may be different because of dust, star formation, and differential age effects. In addition, it is important to realise that although the galaxies which populate $z = 0$ clusters do include those which populate $z = 1$ clusters, the majority would probably be considered “field” objects at the higher redshift. Both the

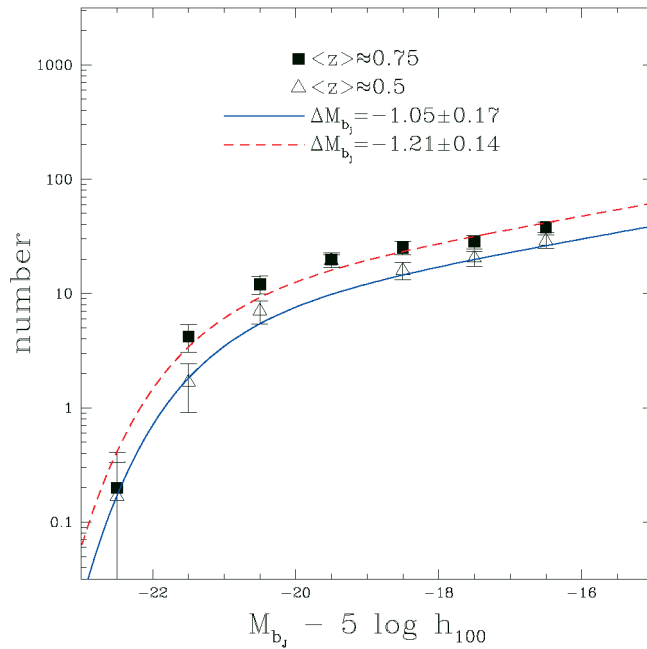


Figure 2: The mean rest-frame b_J -band galaxy luminosity function for all of our $z > 0.6$ clusters (solid points) and for all of our $z < 0.6$ clusters (open points). The blue solid line is the best fit Schechter function to the intermediate redshift sample with α fixed at the local value of -1.28. The red dotted line is the best fit to the high redshift sample, also with $\alpha = -1.28$. The quoted brightening is with respect to the 2dF cluster luminosity function. Figure prepared by Gregory Rudnick.

newly accreted galaxies and the original cluster members may also have their luminosities altered by merging since $z = 1$. Thus, quite detailed modelling is needed in order to interpret the evolution of cluster LFs.

Observations of many local clusters from 2dF Galaxy Redshift Survey (2dFGRS) have shown that the LF of cluster galaxies is remarkably similar for clusters with many different properties (De Propris et al. 2002). We use this large local sample as a zero-point for studying evolution in our own dataset. Using the observed SED of each galaxy, normalized to its total I -band flux, and the spectroscopic redshift of the cluster in which it resides, we derive the rest-frame b_J luminosity. We then use our cleaned cluster galaxy samples to construct a LF for each cluster. To obtain a mean cluster LF in each redshift bin, we stack our clusters. We split our sample at $z = 0.6$ and plot the mean high and intermediate redshift LFs in Figure 2. We determine the brightening of our LFs with respect to the local mean cluster LF from 2dF by fitting with a Schechter function keeping α fixed at the 2dF value of -1.28 and marginalising over the normalization. This results in derived brightenings of $\Delta M_{b_J} = -1.05 \pm 0.17$ at $\langle z \rangle \approx 0.5$ and $\Delta M_{b_J} = -1.21 \pm 0.14$ at $\langle z \rangle \approx 0.75$. This can be compared to the brightening predicted by changing M/L values of ellipticals (van Dokkum & Stanford, 2003), $\Delta M_{b_J} = -0.57 \pm 0.05$ at $z = 0.5$ and $\Delta M_{b_J} = -0.86 \pm 0.08$ at $z = 0.75$. It is interesting that we see a fading of the LF which appears larger than expected just from the aging of stars in early-type galaxies. It is unclear whether this is due to the inclusion of later types in our sample, or to the fact that recently added galaxies are systematically fainter than those al-

ready present in clusters at high z .

The Colour-Magnitude Relation and Galaxy Morphology

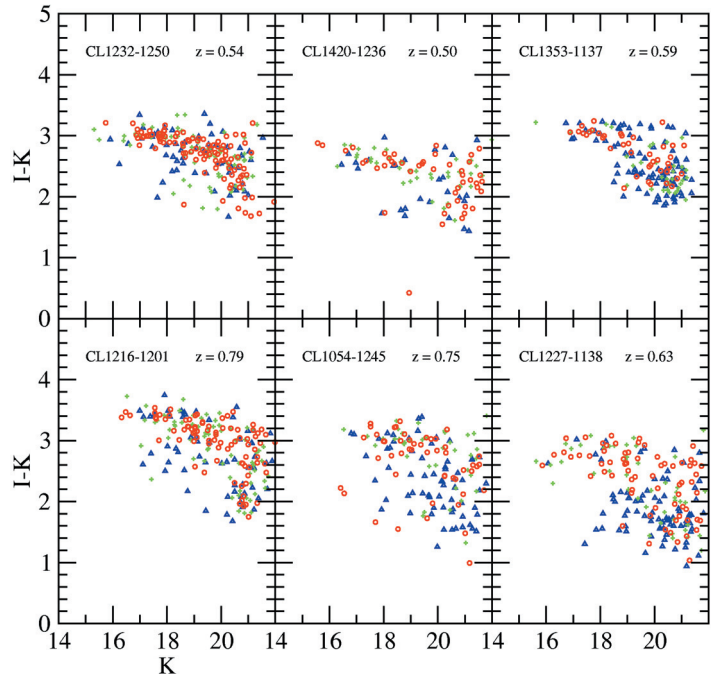
One powerful characterization of the galaxy population is the joint luminosity-morphology-colour distribution. Different morphological components are thought to have different formation mechanisms and the colour of a galaxy results from a combination of its dust content, its SFH, and its metallicity. Most clusters in the local universe have a dominant population of red galaxies which appear uniformly old. These “red sequence” galaxies are spheroid-dominated, but many of them also have a significant red disk. These may be the transformed remnants of infalling spirals. There is also a small population of blue galaxies in clusters, whose fractional contribution to the cluster light increases with increasing redshift (the so called “Butcher-Oemler effect”) and whose low redshift descendants are uncertain.

To study how galaxies are affected by the environments in which they reside, it is necessary not only to go backwards in time, but also to probe a range of environments at each epoch. It is in this area where EDisCS excels. Using our “cleaned” cluster samples we can construct optical/NIR colour-magnitude diagrams with galaxies classified by morphology. Examples are shown in Figure 3. Immediately obvious is the large variation in the red sequence strength. The clusters with a strong red sequence still have significant numbers of blue galaxies, however, although the most luminous galaxies are almost always red. These blue galaxies reflect the Butcher-Oemler effect, and we see its cluster-to-cluster variation clearly.

Figure 3: Colour-Magnitude morphology diagrams for six of our intermediate and high redshift clusters. For each cluster, the colour coding of the points indicates bulge-to-total ratio. Blue triangles are galaxies with $B/T < 0.3$, green plus marks are those with $0.3 \leq B/T < 0.6$, and the red circles are those with $B/T > 0.6$. Note the large cluster-to-cluster variation in red sequence strength as well as the large and variable number of disk-dominated galaxies which lie on the red sequence. Figure prepared by Luc Simard.

Another striking trend is for the relative strength of the red sequence to decrease with increasing redshift, along with the ratio of red to blue galaxies at the bright end. Our spectroscopy will show whether these bright blue galaxies are still actively forming stars or if they are “post-starburst” systems, devoid of current star formation. Either way, these blue galaxies must redden with time so that, by lower redshift, the galaxy populations in these clusters resemble those seen in the local universe.

The excellent quality of our deep VLT images makes it possible to undertake detailed morphological studies. Using the GIM2D code we perform bulge-disk decompositions for all galaxies by fitting seeing-convolved models directly to the 2D images. Extensive Monte Carlo simulations (e.g., Simard et al. 2002) have allowed us to assess where the estimated morphological parameters can be trusted and we should robustly determine the bulge-to-total ratios (B/T) and disk scale lengths for the brighter galaxies in all our clusters. First results are shown in Figure 3, where the differ-



ent points correspond to different B/T values. At all redshifts, the blue galaxies are predominantly disk-dominated. The red sequence, however, shows a large number of disk-dominated galaxies, even in some of our richest clusters. In a few clusters, the disk-dominated galaxies even dominate the red sequence. What are these galaxies? At the bright end, our spectroscopy should tell us whether they are dominated by an old stellar population or by a dusty

starburst.

Even with the high quality of our FORS2 data, detailed morphological classification at $z \sim 0.6 - 0.8$ is difficult, especially for structural parameters of the bulge. To improve the quality of our morphological classification at high redshift, we have obtained 80 orbits of Hubble Space Telescope (HST) F814W data using the Advanced Camera for Surveys (ACS) for 10 of our higher redshift clusters. These data are com-

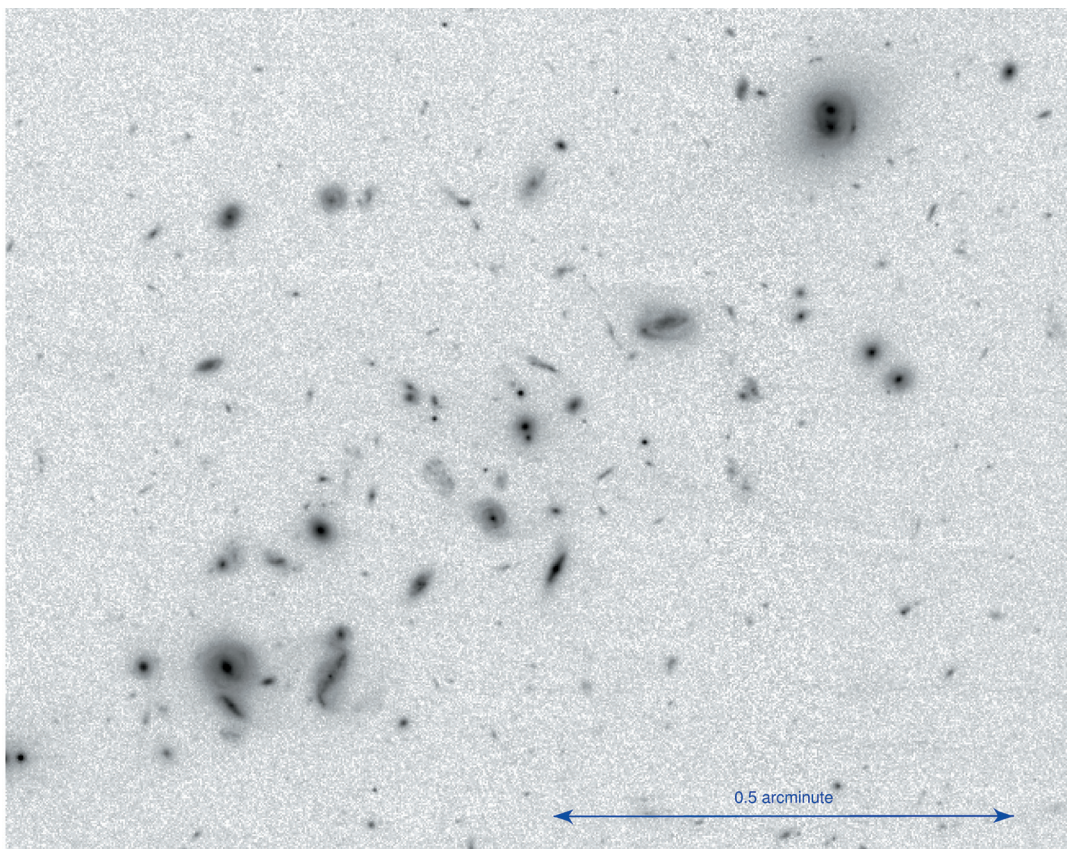
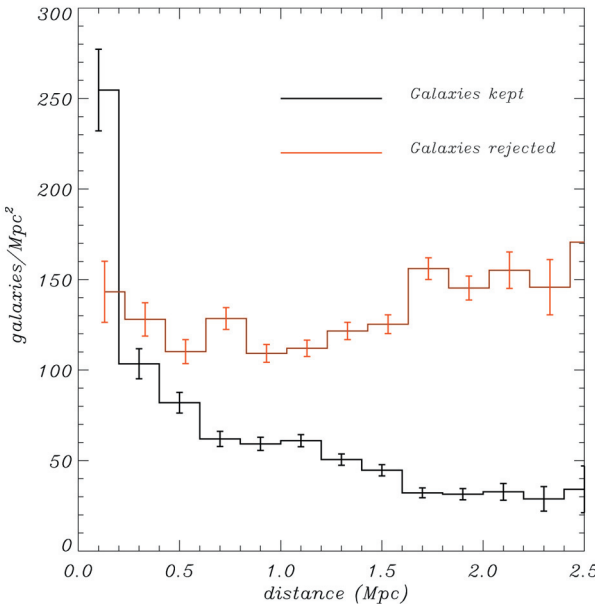


Figure 4: A 5-orbit F814W image of the cluster cl1037-1243 ($z = 0.580$) taken with the Advanced Camera for Surveys (ACS) on board the Hubble Space Telescope (HST). This is one of our lowest redshift candidates imaged with ACS and therefore demonstrates the maximum image detail which we will obtain. The high spatial resolution afforded by these images allows us to measure bulge scale lengths and bulge ellipticities for our highest redshift clusters, as well as to see small-scale structure in many galaxies. By using the ground-based and HST data to constrain the outer and inner regions respectively, we will be able to build a detailed picture of galaxy morphology in our highest redshift clusters. Figure prepared by Vandana Desai.

Figure 5: Stacked radial profile for four clusters with $\langle z \rangle = 0.75$. The black line counts all retained galaxies with $I < 24$, while the red line counts galaxies rejected using photometric redshifts. Note that the rejected galaxies show no concentration to the cluster center (the residual non-flatness is caused by large-scale structure unassociated with the clusters) while the mean cluster profile is detected significantly to 1.5 Mpc. Figure prepared by Gabriella De Lucia.



prised of four one-orbit tiles that cover the same field of view as the deep VLT images, with an additional four orbit central exposure. A reduced image of the center of one of the lowest redshift clusters with HST imaging, the cluster cl1037-1243, ($z = 0.58$) is shown in Figure 4. This image, which comprises five orbits of exposure time, already illustrates the wealth of structure visible, including spiral structure and bars. The apparent lack of bright galaxies with elliptical morphology is also quite striking. With these data, we will be able to derive bulge scale lengths and bulge ellipticities even for our highest redshift clusters.

Cluster Structure

In addition to studying the galaxy populations within our clusters, our large dataset also allows us to study the structure of the clusters themselves. To mitigate cluster-to-cluster variations we stack the clusters in a given redshift range and calculate their mean radial profile. Such an average profile can meaningfully be compared to a similarly stacked profile of simulated clusters to evaluate whether the physical processes which influence galaxy properties as a function of clustercentric distance are correctly modelled in the simulations. In Figure 5 we show the

stacked density profile from four clusters with $\langle z \rangle = 0.75$. Although the individual cluster profiles can be quite noisy, we clearly detect the mean cluster profile out to 1.5 Mpc.

Our study of cluster structure will not, however, be limited to radial profiles. Using our suite of high-resolution simulations of cluster and cluster galaxy formation, we can compare models and observations statistically in the full, three-dimensional space of observables (projected position on the sky + radial velocity). In Figure 6 we compare the projected galaxy density distribution in two observed clusters with simulations. All density maps were similarly constructed by smoothing the discrete galaxy distribution with an adaptive kernel. The input catalogues correspond to a magnitude-limited sample, and, in the observational case, contain only those galaxies which survived our photometric redshift cut. It is obvious from these plots that the detail of the simulations now matches that of the observations, allowing us to compare the two directly using such “mock” catalogues.

Weak Lensing

The depth and image quality of our VLT imaging is so high that we can detect and measure the shapes of many faint background galaxies lying behind our clusters. Gravitational lensing effects due to the matter within the clusters distort these background images causing a weak but measurable tendency for the principal axes of nearby images to align. Measurements of this effect across an image can be inverted to obtain a smoothed map of the pro-

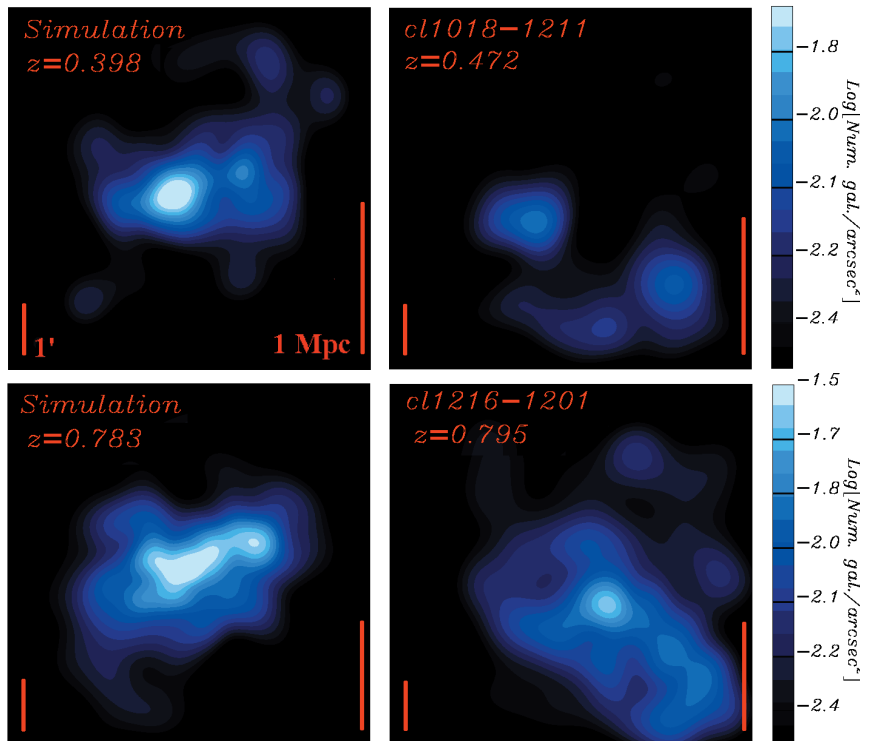


Figure 6: Projected galaxy density maps smoothed using an adaptive kernel technique. The bottom right panel shows our highest redshift cluster cl1216-1201 ($z = 0.795$) and the top right panel shows the cluster cl1018-1211 ($z = 0.472$). All cluster members at $I < 25$ are used. In both clusters, many non-members have been excluded based on photometric redshifts. The panels on the left show projections of two of our high resolution simulations at similar redshifts to the observed clusters. The galaxies in the simulations are selected over the same projected area, accepting only objects within $\pm 2000 \text{ km s}^{-1}$ from the brightest cluster galaxy and applying the same I -band magnitude limit as in the observations. Figure prepared by Gabriella De Lucia.

jected total mass distribution. This can be compared with the projected distribution of cluster light and with the cluster mass inferred using the Virial Theorem and the observed motions of galaxies within the cluster. The precision of such mass estimates from gravitational lensing can be enhanced by using photometric redshifts or color cuts to isolate galaxies which lie behind the cluster. In Figure 1 we show mass surface density contours derived from a weak lensing analysis overlaid on optical images of four of our clusters. At each redshift we show two clusters, both spectroscopically confirmed to have many members, but only one of which shows a clear lensing signal. These results demonstrate yet again the diversity of our sample, highlighting the need for large datasets to correctly characterize the cluster population. When our spectroscopy is fully reduced we will be able to compare the equivalent “velocity dispersion” derived from lensing to that measured from the galaxy velocities, allowing us to check if the clusters are in a relaxed dynamical state. Deviations from such a state are to be expected, given the evident asymmetry of many of our clusters. Comparison with our simulations will check whether deviations from a relaxed state are at the theoretically predicted level.

Spectroscopic Science

The EDisCS project is also distinguished by the abundance of high quality spectroscopy it is assembling. With these data we will explore in detail the physical characteristics of the ~ 800 cluster members, together with a greater number of field galaxies. As shown in Figure 7, our data are good enough to measure the internal kinematics of galaxies down to at least $I = 21.5$. With such spectra we will make field-to-cluster comparisons for fundamental plane and Tully-Fisher evolution, we will determine how the stellar populations in elliptical galaxies evolve with time, we will identify active galactic nuclei, star-forming galaxies and “post-starburst” systems, and we will see how the abundance of all such systems varies with redshift and environment. Because our spectroscopic selection samples all morphological types, we can examine the relations between luminosity, mass, and size for disk galaxies and compare these relations in the cluster environment to those in the field at similar redshift, again providing important constraints for models of galaxy evolution. In combination with our photometric SEDs, the spectral range of our observations will allow us to characterize the stellar populations, SFRs, heavy element abundances, and SFHs of our galaxies. In combination with detailed modelling, we will then be able to build

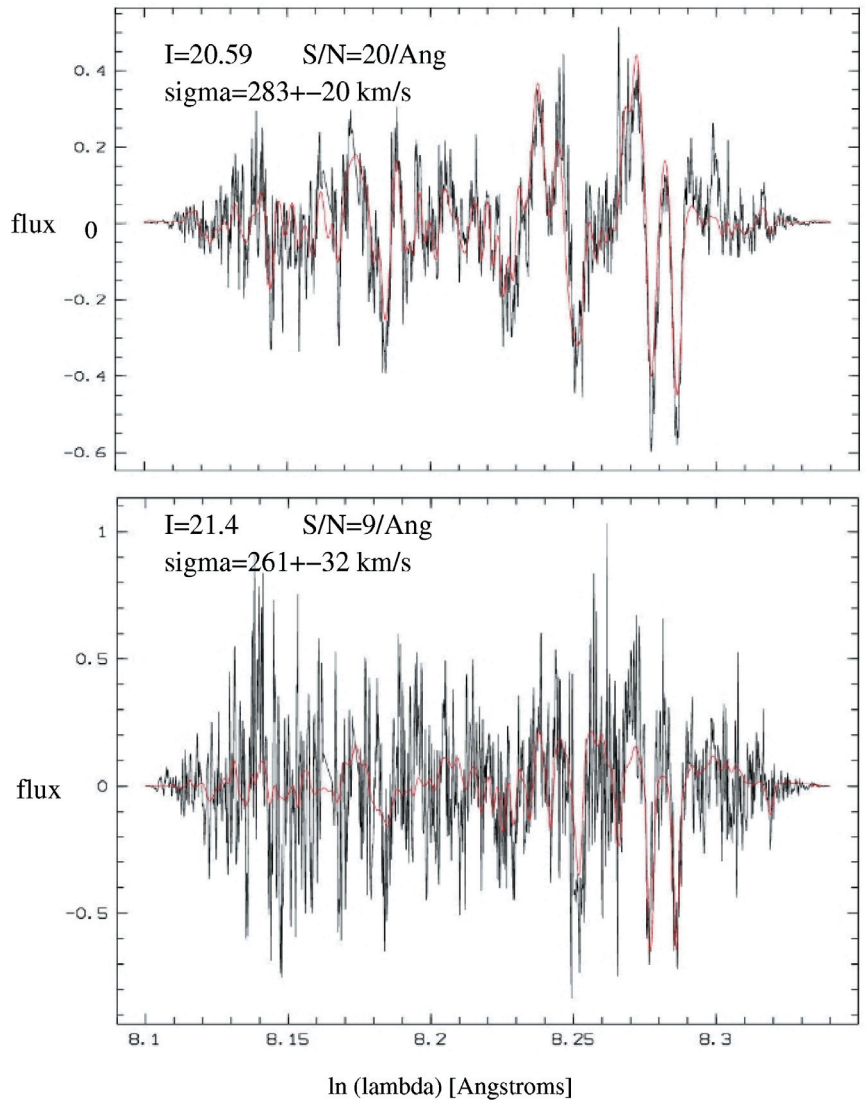


Figure 7: Measures of velocity width for two galaxies in cl1216-1201 at $z = 0.795$. The dark line is the galaxy spectrum with the continuum removed. The red line is the best fit stellar template convolved with the instrumental resolution and a Gaussian velocity dispersion. Using our spectra, we are able to obtain precise velocity dispersion measurements from absorption lines down to $I \sim 21.5$. The instrumental resolution is approx 110 kms^{-1} . Figure prepared by Roberto Saglia.

up a much clearer picture of how galaxy evolution is driven by internal and environmental processes.

Our program has shown that the cluster-to-cluster variance in many cluster properties is large. To obtain a picture of the typical clusters as a function of redshift and environment, and to study the scatter in their properties, it is necessary to study many objects in detail. Thanks to our large and homogeneously selected sample and the high quality of the imaging and spectroscopic data provided by ESO facilities, a comparison of the EDisCS dataset to nearby large cluster samples and to detailed theoretical models will substantially improve our understanding of how galaxies have evolved since the universe was half its present age.

References

- Butcher, H. & Oemler, A. 1978, ApJ, 219, 18
- De Propris et al. 2002, submitted to MNRAS, astro-ph/0212562
- Dressler, A. 1980, ApJ, 236, 351
- Dressler, A. & Gunn, J. E. 1983, ApJ, 270, 7
- Dubinski, J. 1998, ApJ, 502, 141
- Farouki, R. & Shapiro, S. L. 1981, ApJ, 243, 32
- Gonzalez, A. H., Zaritsky, D., Dalcanton, J. J., & Nelson, A. 2001, ApJS, 137, 117
- Gunn, J. E. & Gott, J. R. I. 1972, ApJ, 176, 1
- Larson, R. B., Tinsley, B. M., & Caldwell, C. N. 1980, ApJ, 237, 692
- Moore, B., Katz, N., Lake, G., Dressler, A., & Oemler, A. 1996, Nature, 379, 613
- Simard, L. et al. 2002, ApJS, 142, 1
- Springel, V., White, S. D. M., Tormen, G., & Kauffmann, G. 2001, MNRAS, 328, 726
- van Dokkum, P. G. & Stanford, S. A. 2003, ApJ, 585, 78
- White, S. D. M. 1976, MNRAS, 174, 19